

**Elucidation of the Mechanism for Maintaining Ultrafast Domain Wall Mobility
Over a Wide Temperature Range**

S. Ranjbar^{1}, S. Kambe¹, S. Sumi¹, P. V. Thach^{1,2}, Y. Nakatani³, K. Tanabe¹, H. Awano¹*

¹Toyota Technological Institute, Nagoya 468-8511, Japan

²Institute of Materials Science, Vietnam Academy of Science and Technology, 18
Hoang Quoc Viet, Hanoi, Vietnam

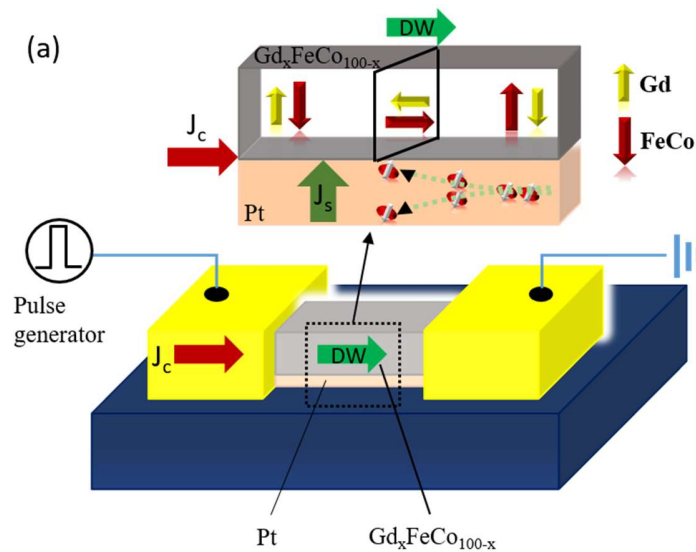
³Graduate School of Informatics and Engineering, University of Electro-
Communications, Chofu, Tokyo 182-8585, Japan

Email: sina.ranjbar@toyota-ti.ac.jp

Contents

- 1. Device and spin-orbit torque (SOT) mechanism**
- 2. Evidence of angular momentum compensation temperature**
 - a) The anomalous Hall effect (AHE) measurement for different GdFeCo compositions.*
 - b) Estimation of T_{AMC} from T_{MC} .*
 - c) Thermal stability*
- 3. Numerical simulation to determine the temperature distribution in nanowire**

1. Device and spin-orbit torque (SOT) mechanism



Supplementary Figure 1. schematic of the Pt/
 $\text{Gd}_x\text{FeCo}_{100-x}/\text{SiN}$ wire structure.

The domain wall (DW) is driven through the wire either by spin-transfer torque (STT) or spin-orbit torque (SOT) mechanism. In the STT system, the charge current is spin-polarized within the ferromagnetic layer, and in the SOT system, the spin-polarized current is produced by SHE in the heavy metal layer (Ta, Pt) and then injected into the ferromagnetic layer, consequently in both systems in a torque utilized on the DWs. Therefore, a large SHE leads to assist in DW motion in RE-TM nanowires. Recently, Ferrimagnet shows the high SOT efficiency ^{[1],[2]}, fast DW motion, low current density J_c and, high mobility ^[3] compared to ferromagnetic materials ^{[4],[5]}.

Supplementary Figure 1 displays a schematic illustration of the Pt/ $\text{Gd}_x(\text{Fe}_{80}\text{Co}_{20})_{100-x}/\text{SiN}$ layer structure and the electrical process to drive DW that exhibits a perpendicular magnetic anisotropy. GdFeCo is a recognized RE–TM ferrimagnetic compound, in which the Gd and $\text{Fe}_{88}\text{Co}_{12}$ moments are coupled antiferromagnetically. The magnetic moment of GdFeCo can be easily controlled by composition or temperature^[6]. Yellow and red arrows present the Gd and $\text{Fe}_{88}\text{Co}_{12}$ sublattice moments in a DW structure, respectively. The sample without the GdFeCo layer has a resistance of 372 Ω , thus the resistivity of Pt is 41 $\mu\Omega$ cm. We estimated the resistivity of GdFeCo within the parallel resistance model. Therefore, the resistivity of the GdFeCo is 169 $\mu\Omega$ cm, which corresponds to the earlier report^[7]. A charge current in heavy metal (Pt) is converted into a spin current (J_s) via spin-orbit coupling and injected into an adjacent ferrimagnet (GdFeCo). The generated spin current in the Pt layer diffused into the GdFeCo layer and assisted DW to move along the current density.

2. Evidence of angular momentum compensation temperature

a) The anomalous Hall effect (AHE) measurement for different GdFeCo compositions.

Supplementary Figure 2(a) displays a schematic illustration of the patterned nanowire with the measurement setup. The width w and length L of the wire was fixed to 3 and 120 μm , respectively. A direct current I ($= 1$ mA) is injected into the nanowire, and transverse voltage is simultaneously measured to obtain the AHE resistance in a

temperature range from 80 to 420 K. Supplementary Figure 2 (b) shows the hysteresis loops of GdFeCo nanowire at various temperature for a different composition. From Supplementary Fig. 2(a) a significant change of resistance is clearly observed by changing the temperature. Therefore, the T_{MC} can determine for all GdFeCo compositions. When the temperature reaches T_{MC} , the net magnetization becomes zero, thus this point is called magnetic compensation temperature.

b) Estimation of T_{AMC} from T_{MC}

In addition, we estimated the angular momentum compensation temperature by the following equations. In GdFeCo total magnetic moment because of two contributions from Gd and FeCo sub-moments can be revealed as:

$$M_{total}(T) = M_{Gd}(T) - M_{FeCo}(T) = \alpha_{Gd}(T_C - T)^{\beta_{Gd}} - \alpha_{FeCo}(T_C - T)^{\beta_{FeCo}} \quad (\text{Eq. 1})$$

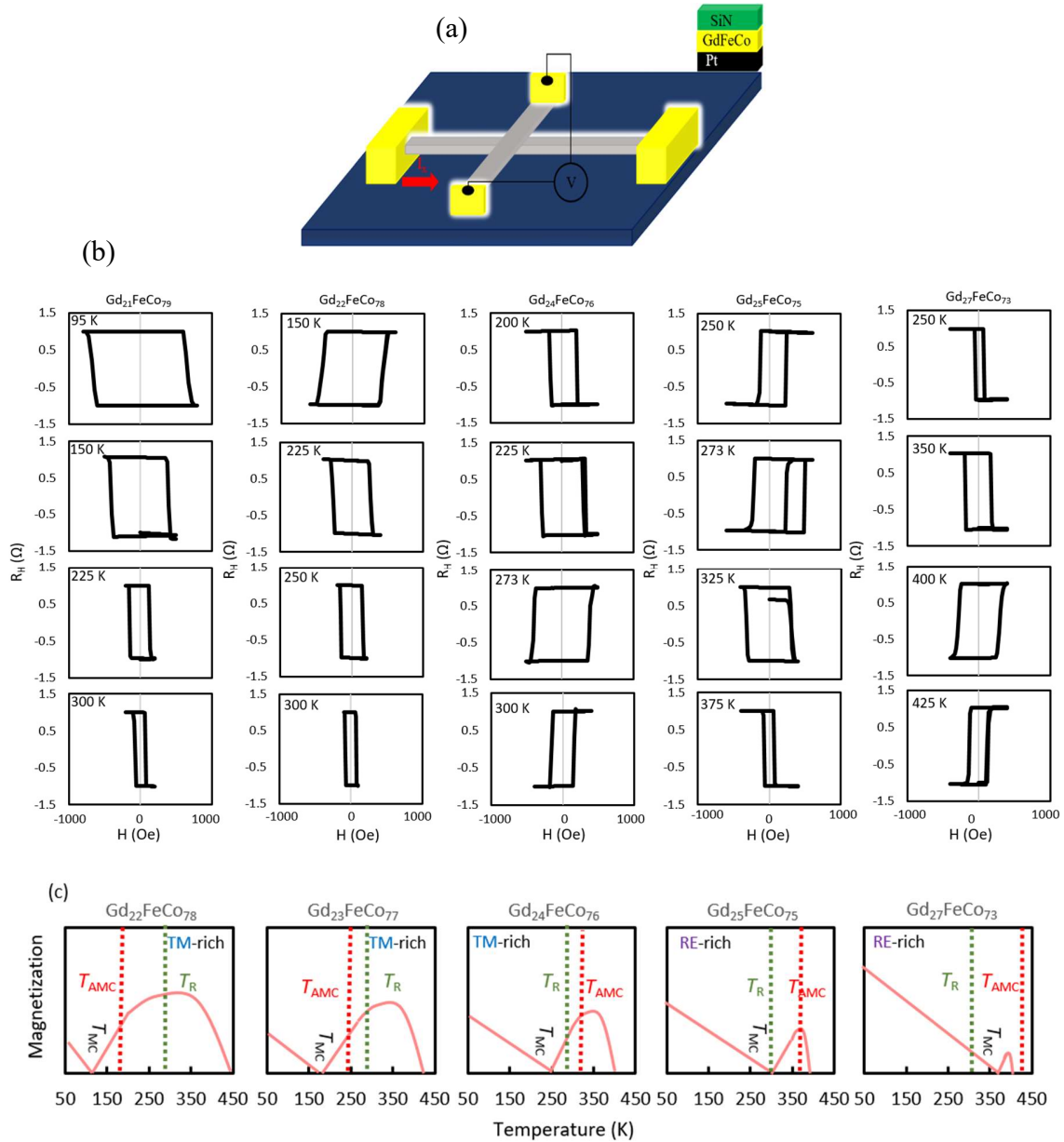
Here α and β are fitting parameters, and T_C is the Curie temperature of GdFeCo.

Note that $\beta_{Gd} > \beta_{FeCo}$ and $M_{Gd}(0) > M_{FeCo}(0)$ ^{[8][9][10]}. When The total magnetic is zero $T_{MC}=T$ hence the equation (1) can be written,

$$T_C - T_{MC} = T_C \left[\frac{M_{Gd}(0)}{M_{FeCo}(0)} \right]^{1/(\beta_{FeCo} - \beta_{Gd})} \quad (\text{Eq. 2})$$

Furthermore, the total angular momentum can be written as,

$$A_{total} = \left[\frac{M_{FeCo}(0)}{\gamma_{FeCo}(0)} \right] \left(1 - \frac{T}{T_C} \right)^{\beta_{FeCo}} - \left[\frac{M_{Gd}(0)}{\gamma_{Gd}(0)} \right] \left(1 - \frac{T}{T_C} \right)^{\beta_{Gd}} \quad (\text{Eq. 3})$$



Supplementary Figure 2. (a) Schematic structure of AHE measurement for all samples, (b) AHE resistance as a function of perpendicular magnetic field for various composition (c) schematic illustration of angular momentum compensation temperature for different GdFeCo composition.

Where $\gamma_i = g_i \mu_B / \hbar$ is the corresponding gyromagnetic ratio, μ_B and \hbar are the Bohr magnetron and Planck constant, respectively. The gyromagnetic ratios of Gd and FeCo components are unequal. When the $A_{\text{total}} = 0$ the following equation can be obtained,

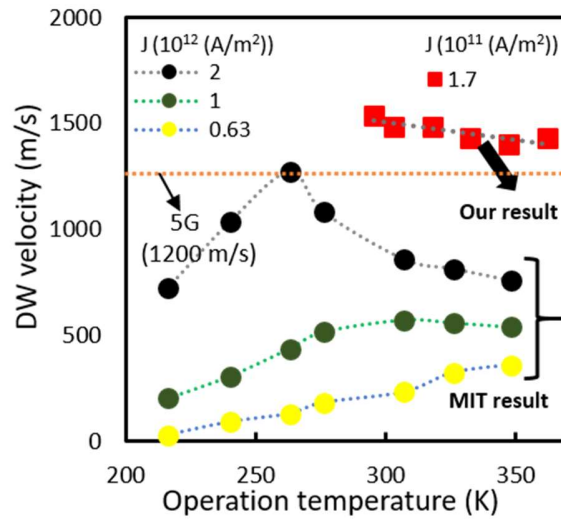
$$T_{AMC} = T_{MC} + T_C \left[1 - \left(\frac{g_{FeCo}}{g_{Gd}} \right)^{1/(\beta_{FeCo} \beta_{Gd})} \right] \times \left[\frac{M_{Gd}(0)}{M_{FeCo}(0)} \right]^{1/(\beta_{FeCo} \beta_{Gd})} \quad (\text{Eq. 4})$$

In order to the previous reports, the g-factors are ($g_{Gd} \approx 2$)^[11] and ($g_{FeCo} \approx 2.16$)^[12]. Consequently, we estimate the T_{AMC} of GdFeCo for different compositions in our study. We summarized this information in the main text of our manuscript (see Fig. 4(c)).

c) Thermal stability

The specification 'industrial-grade wide temperature' is ordinarily determined by the temperature range of 0°C to 55°C^[13]. We should note that defining a wide temperature range for industrial memory applications is crucial. Therefore, finding a fast and thermal stable domain wall motion is crucial in-memory applications. In this section, we compared the thermal stability of Gd₂₄(Fe₈₈Co₁₂)₇₆ with Co₄₄ Gd₅₆, which has been reported by Beach et.al^[4]. Supplementary Figure 3 shows the DW motion as a function of operating temperature for GdCo and Gd₂₄(Fe₈₈Co₁₂)₇₆wires. The GdCo sample reaches its maximum DW speed (1200 m/s) at 260 K and then by increasing the temperature decreases to less than 1000 m/s at high temperature. On the other hand, it is seen that the Gd₂₄(Fe₈₈Co₁₂)₇₆ wire is more fast and stable over a wide temperature range. The current density is 10 times smaller, and the DW velocity is 2 times faster in Gd₂₄(Fe₈₈Co₁₂)₇₆ than that GdCo. This

result proves that the $\text{Gd}_{24}(\text{Fe}_{88}\text{Co}_{12})_{76}$ sample is suitable for designing fast and stable racetrack memory for 5th generation technology.



Supplementary Figure 3. DW velocity as function of operation temperature for GdCo^4 (MIT result) and GdFeCo wires (our result).

3. Numerical simulation to determine the temperature distribution in nanowire

In this section, we simulate temperature distribution in the GdFeCo nanowire after injecting 30ns and 3ns pulse duration. A relationship between a current density and the variation of temperature can be written as the following equation^[14],

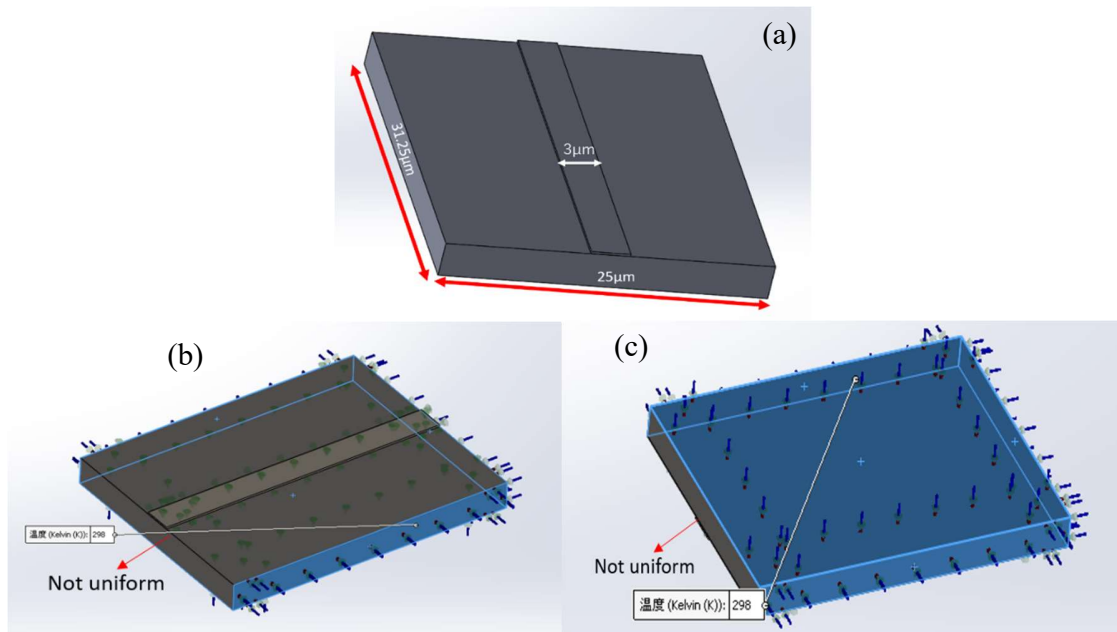
$$\frac{dT}{dt} = \frac{j^2}{C\sigma\rho} \text{ (Eq. 5)}$$

Consider that we assumed a stable current density j , consistent conductivity σ , and initially uniform temperature distribution T . Where ρ is the density [kg/m³], C the specific heat capacity [J/(kg K)], and T the temperature [K].

$$Q = j \cdot E = \frac{1}{\sigma} j^2 \quad (\text{Eq. 6})$$

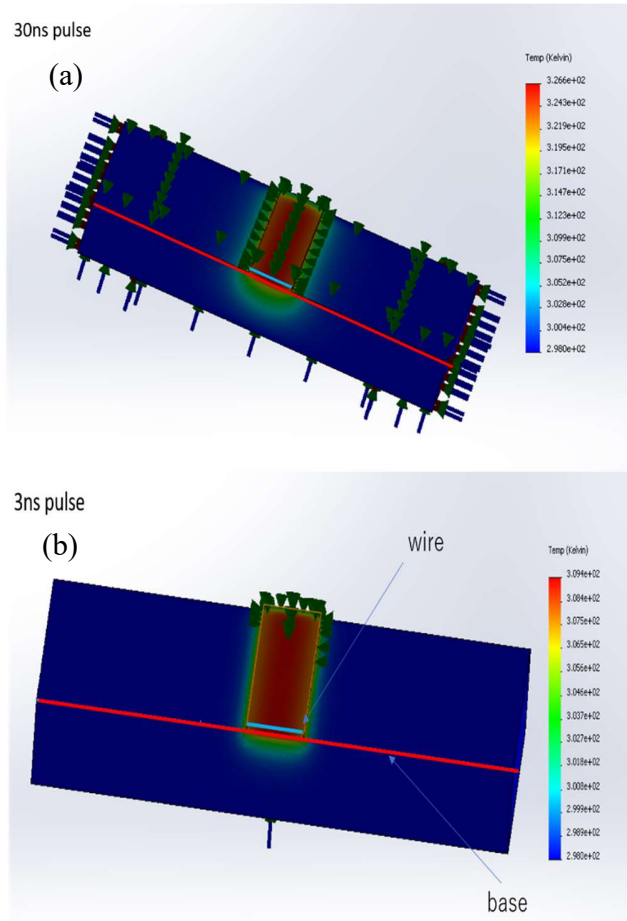
Where σ is the electrical conductivity, Q is a heating term.

Using material parameters for $\text{Gd}_{24}(\text{Fe}_{88}\text{Co}_{12})_{76}$ [$J=1.7 \times 10^{11}$ A/m², Resistance=1378 Ω , initial temperature= 298K, Applied heat:0.338W, thermal conductivity of substrate=1.38 W/(m \cdot K) and Contact resistance= 2.5×10^{-7} (K \cdot m²/W)]. Supplementary Figure 4 (a) shows the model geometry in our study. Piece dimensions are shown in Supplementary Figure 4 (a). Therefore, to complete our simulation we used the following boundary conditions which are shown in Supplementary Figure 4(b-c). The uniform temperature is applied to the blue part of the bar. In this case, we cut the sample at the center of the wire to investigate the temperature distribution at the center of the nanowire. The applied temperature is not uniform at the center of the nanowire.



Supplementary Figure 4. (a) Sample geometry (b-c) cross sectional view of nanowire and substrate for temperature distribution analyze.

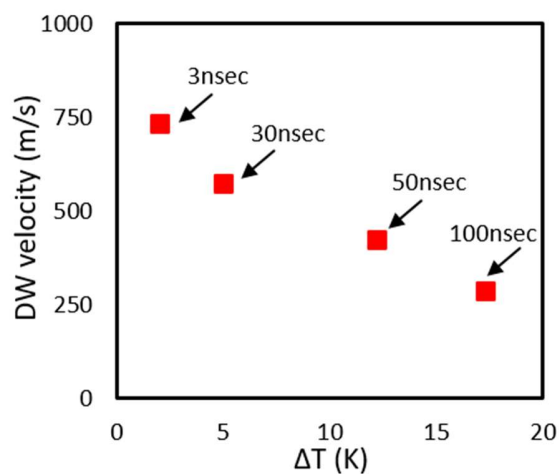
In this section, a current density of $J=1.7 \times 10^{11}$ A/m² is injected into the wire. In this model, we considered 30 ns and 3ns pulse duration to compare the temperature distribution. Supplementary Figure 5 exhibits an overview of the geometry and the computed temperature distribution after 30 ns and 3 ns.



Supplementary Figure 5. Temperature distribution at the center of GdFeCo nanowire and substrate after (a) $t = 30$ ns, (b) $t=3$ ns.

Supplementary Figure 6 shows the DW velocity as a function of temperature gradient (ΔT), besides, the ΔT is related to the temperature difference between the edge and center part of the GdFeCo wire. It is seen that the ΔT is 2 K and 5 K for 3nsec and 30nsec pulse current, respectively. By increasing the pulse width, the temperature gradient increases due

to the Joule heating effect. As a result, the DW velocity decreases linearly by increasing the ΔT , and DW propagation is more uniform and stable when a short pulse current of 3nsec is injected into the GdFeCo wire, which agrees with our finding in the main text (Figure 4(a)).



Supplementary Figure 6. Domain wall velocity as a function of temperature gradient (ΔT) for both 30 and 3nsec pulse current.

References

- [1] J. Yu, D. Bang, R. Mishra, R. Ramaswamy, J. H. Oh, H. J. Park, Y. Jeong, P. Van Thach, D. K. Lee, G. Go, S. W. Lee, Y. Wang, S. Shi, X. Qiu, H. Awano, K. J. Lee, H. Yang, *Nat. Mater.* **2019**, *18*, 29.
- [2] R. Mishra, J. Yu, X. Qiu, M. Motapothula, T. Venkatesan, H. Yang, *Phys. Rev. Lett.* **2017**, *118*, 1.
- [3] S. A. Siddiqui, J. Han, J. T. Finley, C. A. Ross, L. Liu, *Phys. Rev. Lett.* **2018**, *121*, 57701.
- [4] L. Caretta, M. Mann, F. Büttner, K. Ueda, B. Pfau, C. M. Günther, P. Helsing, A. Churikova, C. Klose, M. Schneider, D. Engel, C. Marcus, D. Bono, K. Bagnschik, S. Eisebitt, G. S. D. Beach, *Nat. Nanotechnol.* **2018**, *13*, 1154.
- [5] R. Bläsing, T. Ma, S. H. Yang, C. Garg, F. K. Dejene, A. T. N'Diaye, G. Chen, K. Liu, S. S. P. Parkin, *Nat. Commun.* **2018**, *9*, DOI 10.1038/s41467-018-07373-w.
- [6] I. Radu, K. Vahaplar, C. Stamm, T. Kachel, N. Pontius, H. A. Dürr, T. A. Ostler, J. Barker, R. F. L. Evans, R. W. Chantrell, A. Tsukamoto, A. Itoh, A. Kirilyuk, T. Rasing, A. V. Kimel, *Nature* **2011**, *472*, 205.
- [7] J. H. Kim, D. J. Lee, K. J. Lee, B. K. Ju, H. C. Koo, B. C. Min, O. J. Lee, *Sci. Rep.* **2018**, *8*, 1.
- [8] T. A. Ostler, R. F. L. Evans, R. W. Chantrell, U. Atxitia, O. Chubykalo-Fesenko, I. Radu, R. Abrudan, F. Radu, A. Tsukamoto, A. Itoh, A. Kirilyuk, T. Rasing, A.

- Kimel, *Phys. Rev. B - Condens. Matter Mater. Phys.* **2011**, *84*, 1.
- [9] M. Binder, A. Weber, O. Mosendz, G. Woltersdorf, M. Izquierdo, I. Neudecker, J. R. Dahn, T. D. Hatchard, J. U. Thiele, C. H. Back, M. R. Scheinfein, *Phys. Rev. B - Condens. Matter Mater. Phys.* **2006**, *74*, 1.
- [10] Y. Hirata, D. H. Kim, T. Okuno, T. Nishimura, D. Y. Kim, Y. Futakawa, H. Yoshikawa, A. Tsukamoto, K. J. Kim, S. B. Choe, T. Ono, *Phys. Rev. B* **2018**, *97*, 1.
- [11] Gangulee, R. C. Taylor and A., *J. Appl. Phys.* **1976**, 358.
- [12] G. G. Scott, *Rev. Mod. Phys.* **1962**, *34*, 102.
- [13] E. Farjallah., Monitoring of Temperature Effects on CMOS Memories To Cite This Version : Monitoring Des Effets de La Température Sur Les Mémoires CMOS Présentée Par Emna FARJALLAH, Université Montpellier, **2018**.
- [14] H. Fangohr, D. S. Chernyshenko, M. Franchin, T. Fischbacher, G. Meier, *Phys. Rev. B - Condens. Matter Mater. Phys.* **2011**, *84*, 1.